Vertical mixing of solids in a bubbling fluidized bed

Powder Technology 485 (2027) 123011

Contents lists available at ScienceDirect

Powder Technology

journal homepage: www.journals.elsevier.com/powder-technology

Vertical mixing of solids in a bubbling fluidized bed

M. Díaz-Heras [a,b], A. Siddiqui [c], D. Pallarès [c], J.A. Almendros-Ibáñez [a,b], D.C. Guío-Pérez [c,*]

[a] Universidad de Castilla-La Mancha, E.T.S. de Ingeniería Industrial de Albacete, Albacete, Spain
[b] Universidad de Castilla-La Mancha, Renewable Energy Research Institute, Section of Solar and Energy Efficiency, Albacete, Spain
[c] Chalmers University of Technology, Department of Space, Earth and Environment, Division of Energy Technology, Göteborg, Sweden

HIGHLIGHTS

- Scaling is used to study solids vertical mixing for hot large-scale conditions.
- A novel, pin-probe implementation of magnetic solids tracing is demonstrated.
- Convection is moderately faster than dispersion, with Peclet ranging ~1–5.
- The mixing is less sensitive to fluidization velocity compared to ambient studies.
- Strong impact of the bed height, often overseen in previous literature.

GRAPHICAL ABSTRACT

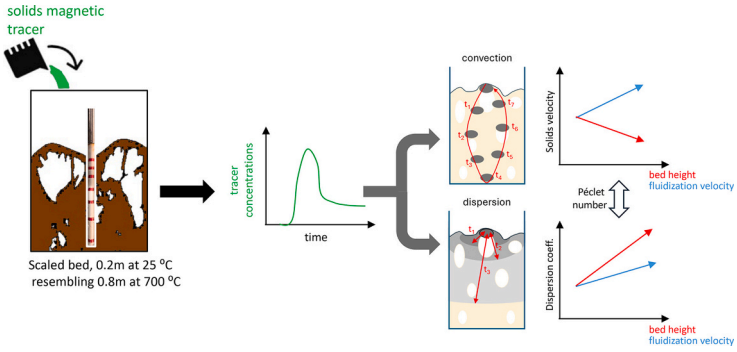

ARTICLE INFO

Keywords:
Solids mixing
Solids dispersion
Solids convection
Magnetic solids tracing

ABSTRACT

This work aims at advancing the understanding of the vertical mixing of bulk solids under conditions relevant for hot operation of large-scale bubbling fluidized beds. A novel implementation of the magnetic solids tracing method is used to sample the transient local concentration of a solids tracer at different heights during batch experiments. The experimental set-up consists of a cold flow model (0.22 m i.d.) operated according to fluid-dynamical scaling laws (yielding the use of 125 μm bronze powder), which allows scale-up of the result data to a virtual large (0.82 m i.d.) bed of 470 μm sand particles operated at 700 °C.

Results indicate that the description of solids vertical mixing cannot be simplified to a purely convective or dispersive process, but a combination of the two. Vertical solids convection acts faster than dispersion for all conditions tested ($u_0/u_{mf} = 1.5–2.5$ and $H_b/d_b = 0.5–1$), with Pe_L-number values ranging between within 1.1–4.6. Increased fluidization velocity enhances both convective and dispersive transport, while increased bed height – a parameter often overseen in previous literature – yields higher dispersion coefficients but lower solids velocity. On up-scaled hot basis, the solids vertical velocity ranges within 0.044–0.12 m/s and dispersion coefficient within 4.9–25 • 10^{-3} m^2/s.

* Corresponding author.
E-mail address: carolina.guioperez@chalmers.se (D.C. Guío-Pérez).

https://doi.org/10.1016/j.powtec.2026.123011
Received 30 October 2025; Received in revised form 22 June 2026; Accepted 23 July 2026
Available online 27 July 2026

1. Introduction

The vertical mixing (also referred to as axial mixing) of bulk solids is a critical aspect in bubbling fluidized beds as it has a relevant impact on the overall chemical potential of heterogeneous reactions and the transport of heat within the bed. In terms of mass transport, the solids vertical mixing governs to which extent the gas-solids contact mode will approach that of countercurrent or not (for low and high mixing, respectively), thus exerting a big impact in the global reaction rate and performance of the heterogeneous reactions in a fluidized bed. In terms of heat transport, the solids mixing plays a key role as it governs the effective heat conductivity of the bed, which is key to the homogeneity or not (for low and high mixing, respectively) of the temperature field. These features are central to the performance of different fluidized bed processes such as the well-established thermochemical conversion of fuels (combustion, gasification, pyrolysis) and cracking, or envisioned applications (e.g. solar radiation receivers in concentrated solar power plants). Given its importance, solids vertical mixing has been a topic of study since the early 1950s [1].

Previous research on the vertical mixing of bulk solids under bubbling fluidization has been eminently experimental, despite the constraints set by the available measurement techniques in terms of either accuracy or resolution. Tracing of the solids phase as continuum by means of chemical (e.g. [2,3]), thermal (e.g. [4]) and magnetic (e.g. [5,6]) methods has commonly been used. Such techniques are based on the assessment of transient properties (concentration, temperature) of batches of solids tracer, thereby providing robust statistics through the many particles involved. However, these techniques are not suitable for determining individual particle trajectories and thus cannot provide direct insight into the underlying mixing mechanisms and complicate the mechanistic understanding of solids mixing. In contrast, particle tracking techniques (e.g. radioactive [7–9] or magnetic [10]) provide time-resolved trajectories of individual particles, from which mixing mechanisms can eventually be studied. By tracking during long periods of time or performing enough repetitions, statistical robustness can be achieved. However, it is often difficult to ensure both that the tracer is detectable and that it keeps the similarity with the bed solids, in which case it is unlikely that the tracer can faithfully mimic the mixing of the bed solids. Literature also reports on experimental works based on visual access to the solids flow in so-called pseudo-2D beds (with a transparent front wall) and applying digital image analysis [11] or in combination with other measurement techniques (like capacitance probes [12]). This approach has a limitation in that the flow pattern established in such beds differs from that in a regular 3D configuration, since the strongly restricted geometry results in weaker bed expansion and slower mixing [13]. Results from such studies can therefore only be used from a qualitative perspective.

The literature regarding vertical mixing of bulk solids in fluidized beds is dominated by works studying beds of Geldart-A solids, due to the focus set for some decades on the development of the fluid catalytic cracking process. For example, Avidan et al. [5] searched for general descriptions that related the vertical dispersion coefficient of bed solids with the operation conditions. They added their own measurements to data gathered from previous literature, all at ambient conditions and covering fluidization velocities up to 1.1 m/s (yielding bed voidages within 0.51–0.7) and for bed diameters within 0.05–1.6 m. This allowed the identification of an increasing trend of the solids dispersion with both the fluidization velocity (roughly linear) and the bed diameter (with slowing growth), with values of the solids vertical dispersion coefficient ranging within 70–150 • 10^{-3} m^2/s.

As fluidized bed technology applications using Geldart-B solids started to develop (for the conversion of solid fuels and the synthesis industry), literature on solids mixing expanded accordingly. Grasa et al. [14] carried out experiments in a pseudo-2D bed of Geldart B-solids, finding dispersion values ranging within 2–30 • 10^{-3} m^2/s. Further, they combined this data with that in previous literature for bubbling beds to derive an expression (Eq. (1)) applicable to both A and B type solids (despite the higher bed voidage and smaller and faster bubbles characterizing the former) and accounting for the excess gas velocity and the size of the particles and the unit.

$$D_{s,vert} = 8.54\ (u_0 - u_{mf}) \left(\frac{d_b\ \nu_g}{u_{mf}}\right)^{0.5} \quad (1)$$

Some more information is available in literature regarding solids axial dispersion, but such data regards flow conditions other than bubbling regime and are therefore out of the scope of the present work, e.g. slugging regime [3] (which exhibits comparatively low dispersion rates, $<10^{-3}$ m^2/s) or the freeboard of a circulating fluidized bed riser [2,9] (where the high gas velocity, 4–8 m/s, and disperse flow condition, 1–10%$_{vol,solids}$, strongly enhance axial dispersion, 10^{-1} to 10^{0} m^2/s). Furthermore, the definition of the parameters studied differs among published works: while most experimental works report the coefficient for macroscopic solids dispersion (thus, at length scales similar to the bubble size), some others analyze the dispersion phenomenon at shorter length scale, thus yielding values in different orders of magnitude. An example of the latter is the work by Migliozzi et al. [12], who combined pressure and capacitance probes to calculate the micro-scale solids dispersion coefficient based on the kinetic theory of granular flow, yielding between 10^{-2} and 10^{-1} m^2/s.

Mathematical modeling has also been used in the analysis of bulk solids dispersion. Salatino et al. [15] used semi-empirical expressions from the classic two-phase flow theory that describes the bubble flow, to estimate the macroscopic solids dispersion coefficient under bubbling conditions to values around 10^{-3} m^2/s. More recently, the development of more reliable first-principle mathematical models and increased computational capacity have led to the development of CFD methods suitable to investigate solids mixing [16], concluded numerically that the vertical mixing rate of solids is somewhat 2-3× faster than that in the horizontal directions [17].

Despite the available data and information, there is a general lack of experimental data regarding the vertical mixing of B-type solids in 3-dimensional units under bubbling regime and at conditions relevant to large-scale operation. For example, while the relative significance of convection and dispersion on the solids vertical mixing in CFB risers has been object of previous study, literature has not analysed this in the bubbling bed region. Further, while the impact of fluidization velocity, particle size and bed diameter on the solids vertical mixing has been studied, that of the bed height remains unexplored although it is shown to strongly affect the solids horizontal mixing [6].

This work aims at studying solids vertical mixing under conditions relevant for hot operation of large-scale bubbling fluidized beds. More specifically, the objectives are: i) to complement existing experimental data with measurements representative for a relatively large geometry and hot conditions, ii) to assess the validity of established literature expressions under such conditions, iii) to assess the contribution of convective and dispersive transport to the solids mixing, and iv) to assess the impact of fluidization velocity and bed height on both these transport modes. To achieve these, this work features a novel implementation of the magnetic solids tracing method, capable of acquiring transient local concentration of a solids tracer at various positions within the bed. Experiments were carried out in a cylindrical fluidized bed operated according to fluid-dynamical scaling laws, allowing for the conversion of the results to recreate the up-scaled conditions in a virtual bed of 0.82 m-i.d. of 470 μm silica sand particles operated at 700 °C.

The main contributions of this work in terms of novelty are: i) the provision of measurement data with both spatial and temporal resolution, in a 3-dimensional unit under conditions representative for hot large-scale operation, ii) the characterization of the solids vertical mixing in terms of convective and dispersive transport rather than a lumped transport rate, iii) the evaluation of the impact of bed height.

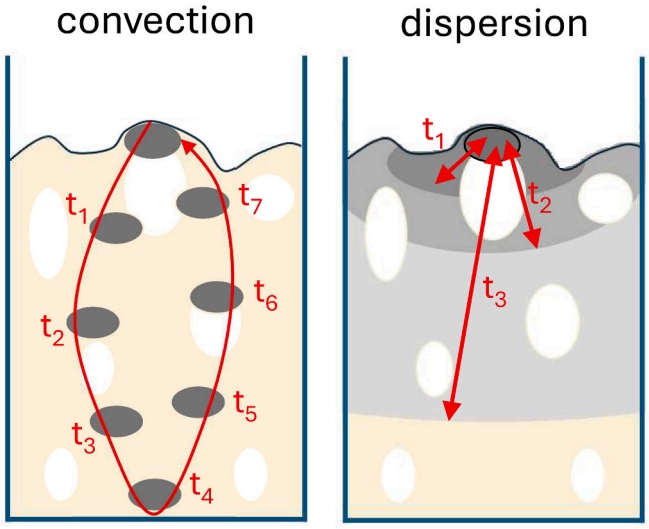

Fig. 1. Conceptual representation of the convective and dispersive transport of a solids batch initially placed at the surface of a bubbling fluidized bed.

2. Theory

The macroscopic mixing of bulk solids in a bubbling fluidized bed can be described as a combination of convective and dispersive transport. Fig. 1 conceptualizes the fate of a small batch of solids injected at the surface of a bubbling bed for two extreme cases: only convective (left-side diagram) and only dispersive mixing (right-side diagram).

The convective mixing in a bubbling fluidized bed follows a macroscopic circulation pattern, sometimes referred to as gulf stream [18]. This flow pattern is induced by the bubble flow, as bubbles drag solids upwards in their wake while rising towards the dense bed surface, consequently creating an equivalent flowrate of bulk solids downwards in the regions not occupied by bubble wakes. This mass balance on the solids phase can be expressed as:

$$\delta_{bub}\, f_w\, u_{s,up} = (1 - \delta_{bub} - f_w\, \delta_{bub})\, u_{s,down} \tag{2}$$

This expression uses the concept of bubble wake fraction, f_w, which represents the fraction of the bubble volume occupied by the wake. Literature reports values of f_w that scatter within 0.3–0.66, with larger units tending to report higher values (see e.g. [10,19]).

The dispersive transport consists of a migration of solids driven by stochastic phenomena such as fluctuations in voidage and velocity and thus evening out concentration gradients with time. Note that dispersion is here assumed to represent the random transport of solids induced by the bed dynamics, resulting in a stochastic transport tending to eliminate concentration gradients. Thus, dispersive solids transport can only be applied for the analysis of systems that, when closed (like the case here of bulk solids in a bubbling fluidized bed), tend to eliminate concentration gradients to eventually reach a state of perfect mixing in the finite domain of analysis. This is the case for our tests according to the measurement data below, which shows an eventual homogeneous distribution of the tracer solids (see measurement data in Section 3.3).

Given a characteristic transport length, L^*, and a characteristic time for each of the transport modes (convection and dispersion), t^*, the parameters characterizing convection (velocity, u) and dispersion (dispersion coefficient, D), are respectively defined as:

$$u = \frac{L^*}{t^*_{conv}} \tag{3}$$

$$D = \frac{L^{*2}}{2\, t^*_{disp}} \tag{4}$$

Rather than being dominated by convection or dispersion (the illustrated cases in Fig. 1), the vertical transport of bulk solid sin a bubbling fluidized results from the simultaneous action of both mechanisms. The separate characterization of each of the two transport mechanisms becomes thus somewhat challenging, as data with both spatial and temporal resolution is required. As detailed in Section 3.3, this work characterizes convection (u in Eq. (3)) by measuring the time it takes for the concentration peak of a batch tracer to travel a certain vertical distance, while dispersion (D in Eq. (4)) is characterized by the time it takes for the injected tracer batch to yield a well-mixed state and the length given by the bed height.

From combining Eqs. (3) and (4), the dimensionless Péclet number can be calculated, which helps in weighing the contributions of convective and dispersive transport:

$$Pe_L = \frac{u\, L^*}{2\, D} \tag{5}$$

Note that definition of the Péclet number as expressed in Eq. (5) is linked to the classic expression for roughly evaluating the significance of axial mixing along a pipe, i.e. $Pe_L = u \bullet L/D$, and differs from that used for studying the extent of cross-sectional mixing, $Pe_d = u \bullet d_b/D$. The latter is derived from the Reynolds number (modified considering the fluid properties through the Schmidt number, $Pe = Re \cdot Sc$) and uses the unit's diameter as characteristic length to study the extent of mixing in the direction across the convective flow, e.g. across the cross section of a pipe. Here it is crucial to note two aspects: i) this work focuses on the mixing along – not across – the vertical convection of solids induced by the bubble flow, and ii) in single-phase flow, the molecular mass diffusion coefficient is an isotropic transport property of the species pair, while the macroscopic solids dispersion studied in this work is strongly anisotropic. Thus, to properly evaluate the relative significance of solids convection vs dispersion in the vertical direction, the solids dispersion in the vertical direction has to be considered specifically (and not approached with the solids dispersion in the lateral direction, which typically differs strongly [17]), and the characteristic length, L^*, must represent the vertical dimension of the domain, i.e. the bed height of each specific run in this work. Referring to classic pipe flow analysis, this is analogous to taking the pipe length, rather than its diameter, as characteristic length when studying the extent of axial mixing along the pipe rather than across it. Note however the importance of keeping track of the type of Pe used to avoid direct comparison of the values for Pe_L and Pe_d.

3. Methodology

3.1. Experimental set-up

The experimental rig was designed and operated according to the Glicksman simplified set of laws for fluid-dynamical scaling [20], which for bubbling conditions sets the following dimensionless parameters to retain flow similarity: $\frac{u^2}{gL}, \frac{u}{u_{mf}}, \frac{\rho_s}{\rho_f}, \emptyset, PSD$. This scaling law set is used in this work to recreate the flow at hot large-scale conditions in a cold flow model more suitable for the use of advanced diagnostics. The main parameters characterizing the experimental cold and virtual hot units are listed in Table 1, together with the scaling parameters and the resulting scaling factors for variables of interest. The model consists of a cylindric bed with an inner diameter of $d_b = 22$ cm, which is fluidized with air at ambient temperature, with bed material consisting of bronze (8492 kg/

Table 1
Main parameters related to the fluid-dynamic scaling used in this work.

	Virtual hot up-scaled unit	Experimental cold flow rig
Temperature	700 °C	25 °C
Bed diameter	0.825 m	0.22 m
Gas	air	air
Solids	Silica sand, 2600 kg/m^3 d_{32} = 470 μm, u_{mf} = 0.145 m/s	Bronze, 8492 kg/m d_{32} = 125 μm, u_{mf} = 0.075 m/s
Fluidization velocity, u_0	0.22–0.36 m/s	0.11–0.19 m/s
Scaling parameters (from [20])		
u_0/u_{mf}	1.5–2.5 (varies with u)	
$Fr = u^2/gL$	0.0059–0.0163 (varies with u)	
ρ_s/ρ_f	7171	
Sphericity, Ø	0.84	
Size distribution	(see *Solids* row above)	
Scaling factors [hot/cold]		
Length [L]	3.75	
Time [t]	1.94	
Velocity [L]/[t]	1.94	
Dispersion coefficient [L]^2/[t]	7.26	

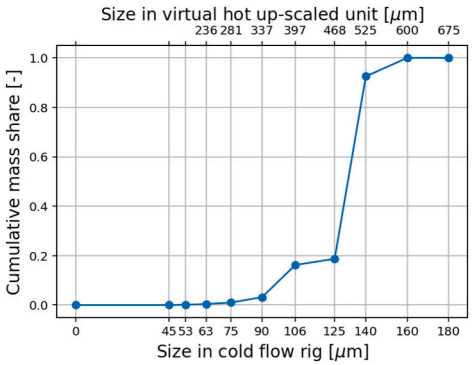

Table 2
Test matrix specifying the values tested for the 2 operational parameters varied (specified also in dimensionless and hot up-scaled basis).

	Values tested
Fluidization velocity, u_0	0.11–0.15–0.19 m/s (u_0/u_{mf} = 1.5–2-2.5) (u_0^{hot}: 0.22–0.29-0.36 m/s)
Bed height, H_b	0.11–0.165–0.22 m (H_b/d_b = 0.5–0.75-1) (H_b^{hot}: 0.41–0.615-0.82 m)

m^3) powder with a Sauter diameter of d_{32} = 125 μm (measured through sieving, and yielding a slightly larger mass-based median size, 131 μm) and sphericity 0.84 (measured using a Malvern Morphologi 4 system). According to the scaling, the cold flow model used in this work resembles a virtual 0.82 m-i.d. bed of silica sand particles (d_{32} = 470 μm, 2600 kg/m^3) operated with air at 700 °C. This specific set-up (of unit geometry and size, temperature, and gas-solids combination) does not correspond to a specific hot unit but is conceptualized to yield representative industrial-scale hot conditions for the solids mixing in fluidized beds for thermochemical conversion.

The use of fluid-dynamic scaling laws yields cold experiments involving smaller beds of finer and heavier solids, resulting in faster dynamics than those observed at large scale with regular solids. This is seen in the scale factors: note that the virtual hot large-scale scale unit and the bubbles it hosts are 3.75× larger than the ones in the cold experiments, while velocities scale with the root-square of that factor, 1.94×. This yields longer characteristic times in the virtual hot large unit, e.g. the much larger bubbles will rise faster, but due to the much taller bed will yield longer rising times (see the 1.94× time scale factor). Further, combination of these scale factors yields a dispersion coefficient 7.26× higher at hot large-scale conditions, due to the bubbles being both larger (3.75×) and faster (1.94×).

A total of 9 different operational conditions were tested, consisting of combinations of 3 bed heights, corresponding to bed aspect ratios (H_b/d_b) of 0.5, 0.75, and 1.0, and 3 fluidization velocities corresponding to fluidization numbers (u_0/u_{mf}) of 1.5, 2.0 and 2.5 (as indicated in Table 2). The use of higher fluidization velocities was prevented by the set-up, but the fluidization numbers here investigated are within the typical range for certain fluidized bed applications such as their use as CSP receiver where operation at $u_0/u_{mf} \leq 3$ is targeted [21]. To ensure robustness of the sampled data experiments were carried out in triplicate. The minimum fluidization velocity of the bronze particles used as bulk solids was determined to be u_{mf} = 0.075 m/s by means of pressure drop measurements at varying fluidization velocity. Note that u_{mf} used in this work for the resembled hot conditions is up-scaled from the cited experimental value (yielding 0.145 m/s), while calculations with classical correlations yield values around 0.09–0.1 m/s. This discrepancy between correlations and experimental values is typically done to the size and geometry distribution of the particles, and occurs also for the bronze particles tested (for which calculations yield u_{mf} = 4–5 m/s while experiments give 0.075 m/s).

This work uses time resolved measurements of local tracer concentrations. For this purpose, the already established magnetic solids tracing technique (MST, see [6] for details) was selected, which employs impedance changes in a coil to quantify the concentration of ferromagnetic material (tracer) in the sensed volume. The impedance signal acquired has a linear relation to the concentration of ferromagnetic solids tracer which is used to build individual calibration lines for each coil. The ferromagnetic powder used as tracer material is an iron-based alloy (FeSi 68 HQ) that has similar physical properties (93 μm, 7028 kg/m^3, sphericity 0.86) to those of the bronze used as bulk solids. Unlike previous implementations of the MST technique [6], where global concentrations in a defined cross section were assessed, in this work local concentrations are measured by means of small coils designed and assembled along a thin (1 cm-i.d.) pin probe shown in Fig. 2. Each coil assesses the tracer concentration of its immediate surroundings, with a sensing volume of approximately 2 cm^3 where sensitivity decays with distance from the coil at a rate of $\propto r^{-2.5}$. By vertically inserting the pin

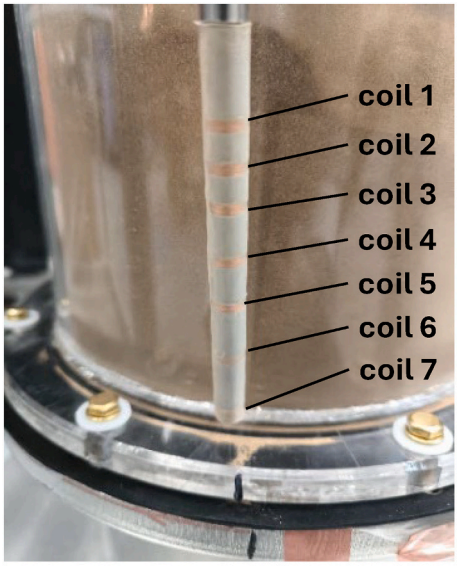

Fig. 2. Arrangement of the magnetic solids tracing system used to measure the solids tracer concentration.

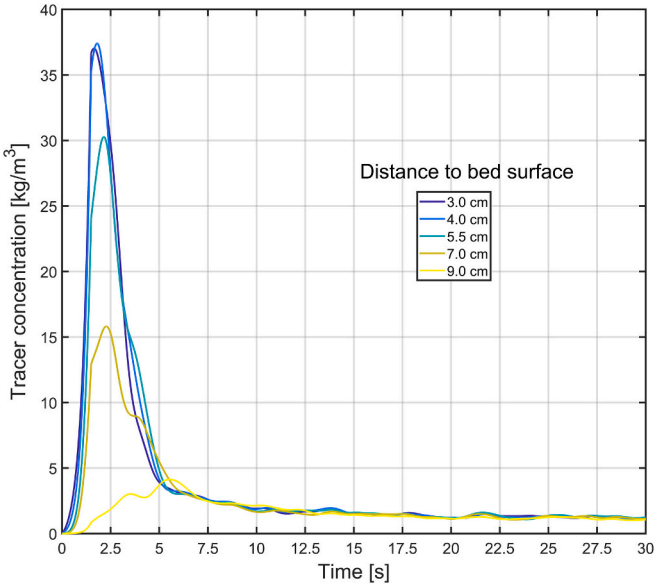

Fig. 3. Transient tracer concentrations measured at five different distances from the bed surface (coils 2 to 6). Data for case $u_0/u_{mf} = 1.5$, $H_b/d_b = 1$.

probe in the bubbling bed, local concentration can be simultaneously acquired at 7 different axial positions (position of the coils along the pin, as indicated in Fig. 2).

3.2. Experimental procedure

Before starting the test, the pin probe is fixed along the vertical centerline of the bed. The test procedure was initiated by establishing steady fluidization conditions in the bed. Then the vertical location of the pin probe was adjusted so that the top coil ended in average 2 cm below the dense bed surface (see Fig. 2). Thereafter, the logging of the coils signal was started, and 20 s of data were collected to later calculate the background concentration. Then, a batch of 200 g of ferromagnetic tracer solids was deposited at the center of the dense bed surface by means of an injection probe (a tube of 17 mm i.d.) without disturbing the fluidization. After that, data was logged for 120 s (for $Hb/d_b = 0.5$) and 180 s (for $Hb/d_b = 0.75$ and $Hb/d_b = 1$) to ensure that the full mixing of the tracer was achieved. While keeping the same fluidization conditions, a new logging was started, and a new tracer batch was deposited on the bed surface to perform a repetition. In total 3 repetitions were done per set of conditions. To prevent the coils from becoming saturated with tracer solids, these are removed with a magnetic separator every third run (corresponding to approximately 600 g of tracer solids).

3.3. Data processing

Fig. 3 exemplifies the transient concentrations of solids tracer measured by five coils at different distances from the dense bed surface (corresponding to coils 2–6 in Fig. 2). The solids concentration data is sampled at 100 Hz and filtered through a moving average with a window of 0.5 s in order to attain smoother gradients that allow for later data processing (as discussed in relation to Fig. 4 below) and improve data representation in the figures here shown; it is however checked that no significant peak shift is introduced by the data filtering. Further, the top and bottom coils (coils 1 and 7, respectively) have been excluded from the analysis, since they were not continuously measuring a representative region of the dense bed in terms of solids concentration: the top coil ended up above the dense bed due to the oscillating bed surface level, while the bottom coil was too close to the gas distributor and measured high voidages related to the inlet gas jets. As seen, the signal from all coils continuously immersed in the bed and far enough from the inlet gas jets converged to the same tracer concentration value at steady state. This stabilization of the sampled tracer concentration at a same value, which is observed for all repetitions of all operational cases, indicates that the solids tracer yields a well-mixed steady state with the bulk solids, which supports the validation of the solids tracer effectiveness in mimicking the bulk solids.

As seen in Fig. 3, the peak in tracer concentration shifts in time and becomes wider according to the distance of the coil to the dense bed surface (where the tracer is injected), suggesting further penetration of the tracer solids with time, and dispersion of the tracer as it moves downwards, i.e. vertical mixing. Also, during the transient state the sum of the concentrations measured at a given time decreases as the tracer is transported downwards, presumably due to mass transport in the lateral direction. The use of a transient dispersion model to analyze the data in Fig. 3 was attempted but was not possible, indicating the need to also consider convection for describing the vertical transport of the solids.

The velocity for the convective vertical transport can be calculated as the velocity at which the concentration peak moves. To obtain the most statistically robust and representative value, this velocity is calculated using data from the coil located farthest from the injection point and still showing a distinct peak, as this is where the signal reflects the most integrated and well-developed flow history. With this, solids downwards velocity is calculated as the distance of the chosen coil to the bed surface divided by the time of peaking (see Eq. (3)).The dispersion coefficient is calculated with Eq. (4) based on the time it takes for the system to reach the well-mixed state, and taking the bed height as the characteristic length. The time required to reach well-mixed state is calculated based on the transient concentration measurements of the bottom-most valid coil (i.e. not affected by the gas jets from the gas distributor). The well-mixed state is achieved when the modulus of the time derivative of the tracer concentration reaches a predetermined threshold value (in this work, data analysis showed 0.5 kg/m^3s to be a value which yielded robustness in the characteristic dispersion time over the different test

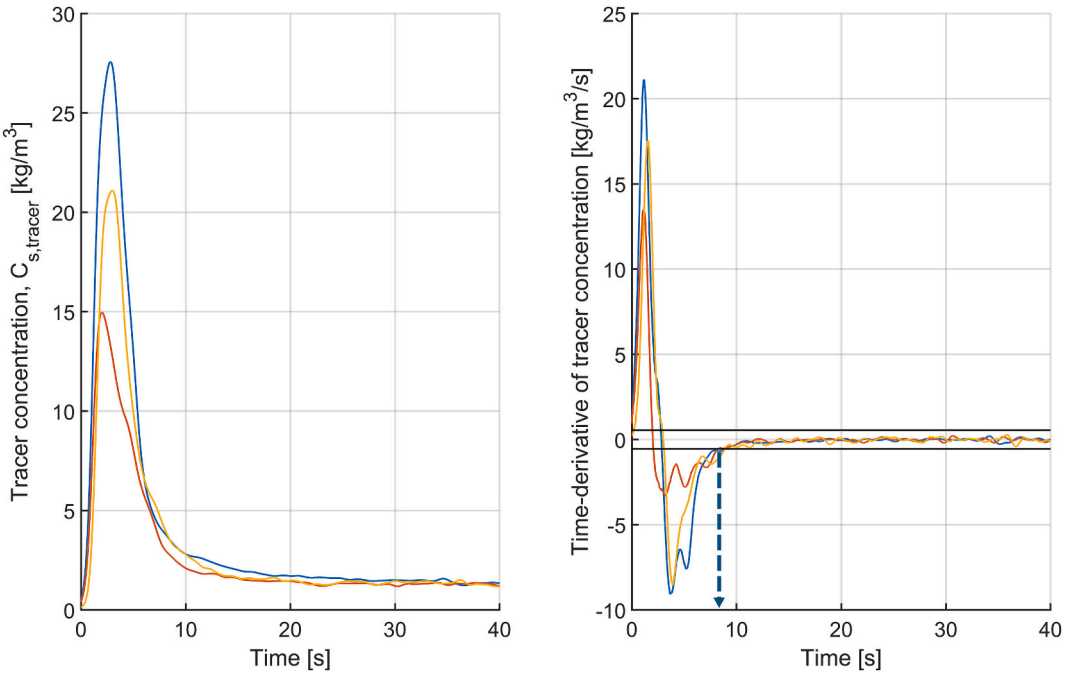

Fig. 4. Experimental data sampled by coil 6 during three repetitions. The blue arrow in the left figure represents the characteristic time for dispersion. Data for case $u_0/u_{mf} = 2.5$, $H_b/d_b = 1$. (For interpretation of the references to colour in this figure legend, the reader is referred to the web version of this article.)

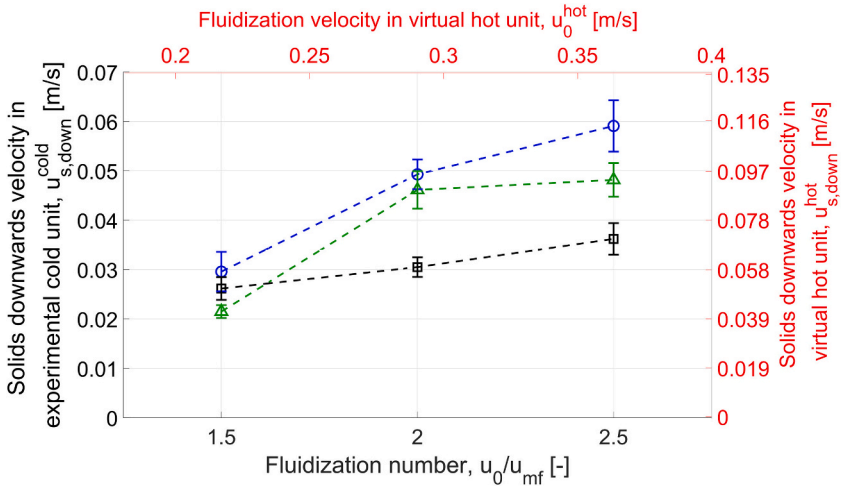

Fig. 5. Solids vertical velocity as a function of the bed aspect ratio (H_b/d_b) or the fluidization velocity under resembled hot conditions. The red auxiliary axes represent the up-scaled values for the 0.82 m-i.d. unit operated at hot conditions. Bars indicate the standard deviation among the values obtained from three experimental repetitions. (For interpretation of the references to colour in this figure legend, the reader is referred to the web version of this article.)

Table 3
Ranges of solids upwards velocity in the resembled hot operations (calculated from the measured solids downwards velocity with Eq. (2), and with f_w = 0.3–0.66). Values in parenthesis indicate the ratio of the solids upwards velocity estimated with $f_w = 0.63$ to the calculated bubble rise velocity.

		Fluidization velocity, u_0		
		0.22 m/s	0.29 m/s	0.36 m/s
Bed height, H_b	**0.41 m**	0.28–0.67 (72%)	0.46–1.12 (105%)	0.55–1.35 (116%)
	0.62 m	0.2–0.49 (45%)	0.43–1.05 (83%)	0.45–1.1 (80%)
	0.82 m	0.24–0.6 (48%)	0.28–0.7 (45%)	0.34–0.83 (54%)

repetitions, as exemplified by the data from the three repetitions shown in Fig. 4b). To exemplify the procedure, Fig. 4a shows the transient tracer concentration curves sampled by the bottom-most coil during the three repetitions of the same experiment (operational conditions u_0/u_{mf} = 2.5, $H_b/d_b = 1$). The time derivative is shown in Fig. 4b, together with horizontal black lines marking the threshold value used to determine the achievement of well-mixed state. The three repetitions of the experiment provide similar values of the characteristic time for dispersion (around 8–9 s for the specific operational conditions plotted).

4. Results and discussion

The results concern the two main variables used here to characterize the solids transport in the vertical direction. On one hand, the solid vertical velocity, indicator of the convective transport, and on the other

hand, the dispersion coefficient, used to quantify the dispersive transport.

Fig. 5 shows the mean solids downwards velocity for the nine operational conditions investigated, i.e. as a function of the fluidization velocity and the bed aspect ratio. The auxiliary top and right axes (in red) correspond to values on a hot up-scaled basis (this is, scaled up according to the corresponding scaling ratios, see Table 1). As seen, the solids downwards velocity increases with the fluidization velocity (expressed as fluidization number), yielding a maximum value slightly above 0.11 m/s for the hot up-scaled unit at a fluidization number of 2.5. Instead, increasing the bed height (expressed in terms of the bed aspect ratio) results in a decrease of the solids velocity.

There is no relevant literature data to compare the downwards velocity data in Fig. 5 to, but the increase with fluidization velocity is expected as bubble activity (volume fraction, velocity and size) is increased and thereby solids convection too. It is though unexpected to observe a decrease of the solids velocity with bed height, as taller beds induce bubble coalescence and larger and faster bubbles, which should also enhance solids velocity.

The upwards convection of solids in the wake region of rising bubbles could not be experimentally investigated due to the difficulties in achieving an enough non-invasive and fast injection of tracer solids at the bottom of the bed. Instead, the mean solids upwards velocity was calculated with the mass balance expressed by Eq. (2), yielding the values reported in Table 3 for the resembled hot operation conditions. The values in Table 3 are given as a range corresponding to the values for f_w reported in literature (f_w = 0.3–0.66), illustrating the strong dependency on this uncertain parameter. Additionally, the table reports in parenthesis for each condition the ratio of the solids upwards velocity (estimated using $f_w = 0.63$, a value claimed to be representative for hot conditions [22]) to the mean bubble rise velocity (calculated with the classical correlations by Darton et al. [23] for bubble growth and Davidson and Harrison [24] for bubble velocity).

The data in Table 3 reflects the strong sensitivity of the conversion between downwards and upwards solids velocity (i.e. Eq. (2)) on the highly uncertain wake region factor, f_w. Further, note that Table 3 contains two cases for which the value of the solids upwards velocities estimated with $f_w = 0.63$ is higher than the calculated bubble rise velocity (i.e. in-parenthesis values beyond 100% in Table 3), which is unphysical. This illustrates, besides the inherent uncertainty of the expressions for bubble size and velocity, the invalidity of extrapolating f_w values between different experimental set-ups and the risks of making direct generalized use of literature values for this parameter. While noting this, qualitative trends from the values in Table 3 can however still be analysed. As seen, as the bed height is increased, the solids upwards velocity decreases in relation to that of the bubbles, possibly indicating that the bubbles in taller beds are less efficient in holding the solids in their wakes and instead lose them to the surrounding. This lower efficiency of the wake regions in withholding solids would in its turn imply an increased lateral and axial dispersion of the solids, as solids leaving the wake will move laterally and join the downwards solids emulsion or a new bubble wake. Thus, this suggests that a single value of the wake factor, f_w, cannot be representative for the different conditions tested, and that taller beds tend to yield lower values of this factor.

Table 4
Péclet number as a function of the fluidization number (u_0/u_{mf}) and bed aspect ratio (H_b/d_b).

$Pe_L = \frac{u L^*}{2 D}$		Fluidization number, u_0/u_{mf}		
		1.5	2.0	2.5
Bed aspect ratio, H_b/d_b	**0.50**	2.9	4.6	2.9
	0.75	1.8	2.5	1.6
	1.00	1.3	1.1	1.5

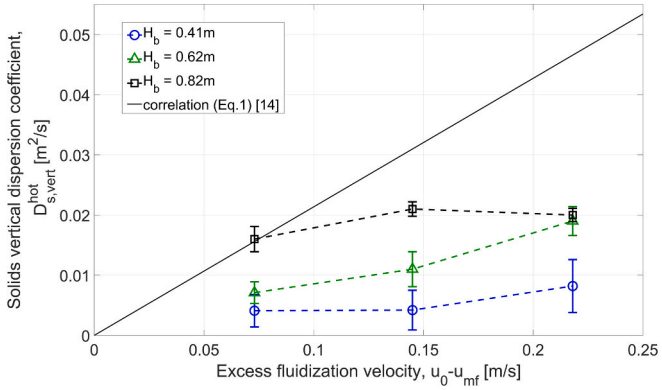

Fig. 7. Solids vertical dispersion coefficient in the resembled hot unit as a function of the excess fluidization velocity and bed height. Experimental data (markers) are compared to the literature correlation [14] given in Eq. (1) (solid line). Bars indicate the standard deviation among the values obtained from three experimental repetitions.

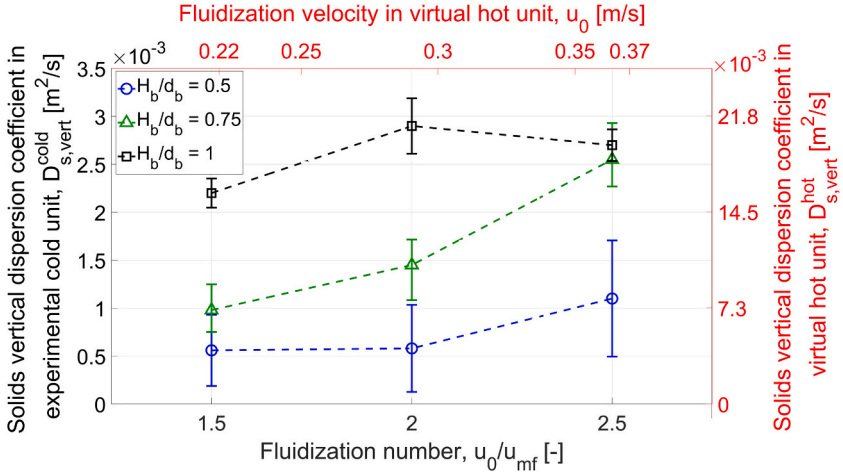

Fig. 6. Solids vertical dispersion coefficient as a function of the fluidization velocity and bed aspect ratio (H_b/d_b). Red auxiliary axes represent the up-scaled values for the 0.82 m-i.d. unit operated at hot conditions. Bars indicate the standard deviation among the values obtained from three experimental repetitions. (For interpretation of the references to colour in this figure legend, the reader is referred to the web version of this article.)

Fig. 6 presents the solids vertical dispersion coefficient as a function of the fluidization velocity and the bed aspect ratio. Similarly to Fig. 5, the auxiliary top and right axes (in red) indicate the values on a hot up-scaled basis (see Table 1). It is observed that an increase of the fluidization velocity attains an enhancement of the solids vertical dispersion rate. The dispersion coefficient in the cold flow model takes values in the order of magnitude of 10^{-3} m^2/s, which are in line with modeling estimations by Salatino et al. [15]. At hot up-scaled conditions the dispersion coefficient reaches up to 0.2 m^2/s. Contrary to the case of the convective transport discussed in Fig. 5, an increase in bed height results in increased dispersive mixing. This aligns with the above discussion on the lower efficiency of the bubble wakes in tall beds to withhold solids, yielding lower upwards velocity and an increase in the vertical dispersion instead.

In order to assess the relative significance of convective and dispersive transport of solids in the vertical direction, the axial Péclet number, Pe_L, is calculated and presented in Table 4 for all tested conditions. For all the operational conditions tested, the values were found to be >1 (ranging within 1.1–4.6), which indicates a generally faster rate of convective transport than that of the dispersive transport. However, since both mechanisms are in the same order of magnitude, there is not a single clearly dominant transport mechanism. Regarding the impact of operational parameters, an increased bed height decreases the relative significance of convection, which was observable from data in Figs. 5 and 6 as higher beds yield both lower solids velocity and higher solids dispersion. The increase of the fluidization velocity; however, does not reveal any clear trend on the dispersion-convection balance, as both transport mechanisms increase. Due to the lack of literature exploring the bulk solids transport under bubbling conditions as separate convection and dispersion mechanisms, the value range $Pe_L = 1.1–4.6$ reported in Table 4 cannot be compared to other works under bubbling conditions. Literature provides Pe_L-values only for experiments in the freeboard of a CFB riser [2], where the value range observed is similar: $Pe_L = 2–9$.

Fig. 7 compares the correlation formulated by Grasa et al. [14] (Eq. (1)), which considers experimental data from 12 different works to our values of solids vertical dispersion. As seen, the results from the present work are in all cases lower than those predicted by the correlation, in average by a factor of 3.2. However, this deviation is still in the range of agreement of the correlation as the literature values considered to derive it scattered considerably (probably due to the wide scope covered, which included both A and B type solids). It is worth mentioning that the results from the present work are consistently similar to those measured by Norouzi et al. [8], who also used type B solids. Further, as observed in Fig. 7, the present work indicates a lower impact of the fluidization velocity (as compared to the generalized correlation), while highlighting the important role of the dense bed height, typically overlooked in previous studies and in Eq. (1).

5. Conclusions

This work studies the vertical mixing of bulk solids in a bubbling fluidized bed, by evaluating local transient concentrations of a magnetic tracer material. For this purpose, the work implements the magnetic solids tracing method using small inductance coils arranged along a thin pin probe. The work uses fluid-dynamic scaling so that results derived from measurements in the cold flow model used can be scaled-up to represent a 0.82 m-i.d. hot unit (700 °C) operated with silica sand and air.

Measurements show that solids downwards convection increases with fluidization velocity and decreases with bed height. Regarding the latter, calculations indicate that the solids upwards velocity is significantly lower than the bubble rise velocity for taller beds, suggesting that the bubble wakes in such beds are more prone to exchange solids with the surrounding emulsion, thus yielding lower convective transport and increased dispersive one. This is confirmed by result data on showing increased solids dispersion with bed height – and with fluidization velocity, as expected. For the hot up-scaled conditions, the solids vertical dispersion coefficient yields values within the range 4–21 • 10^{-3} m^2/s, while the solids downwards velocity attains 5–11 • 10^{-2} m/s. Further analysis of the data in terms of the Péclet number indicates that for the conditions investigated convective solids transport is generally faster than dispersion, although both mechanisms remain in the same order of magnitude and are thus of relevance ($Pe_L = 1.1–4.6$).

These results resembling hot conditions follow a similar qualitative trend of increased solids dispersion with fluidization velocity, although with less impact than that reported by previous literature. The results of this study highlight the significant impact of bed height on the convective and dispersive vertical transport of solids in bubbling beds of Geldart B type.

Nomenclature

$C_{s,tracer}$	Concentration of solids tracer [kg•m^{-3}]
$D_{s,vert}$	Solids vertical dispersion coefficient [m^2•s^{-1}]
d_{32}	Sauter diameter of the solids [m]
d_b	Bed diameter [m]
f_w	Volume fraction of wake region relative to bubble [−]
Fr	Froude number [−]
H_b	Bed height[m]
L^*	Characteristic length [m]
Pe	Péclet number [−]
Sc	Schmidt number [−]
t	time [s]
t^*	Characteristic time [s]
u_0	Fluidization velocity [m•s^{-1}]
u_{mf}	Minimum fluidization velocity [m•s^{-1}]
$u_{s,down}$	Downwards velocity of the solids [m•s^{-1}]
$u_{s,up}$	Upwards velocity of the solids [m•s^{-1}]
δ_{bub}	Volume fraction of bubble phase in the bed [−]
ν_g	Kinematic gas viscosity [kg·m^{-1}·s^{-1}]
$Ø$	Solids sphericity [−]

Superscripts

cold	measured at ambient conditions
hot	up-scaled to hot large-scale conditions

CRediT authorship contribution statement

M. Díaz-Heras: Writing – review & editing, Methodology, Investigation, Funding acquisition, Formal analysis, Data curation, Conceptualization. **A. Siddiqui:** Writing – review & editing, Methodology. **D. Pallarès:** Writing – review & editing, Writing – original draft, Supervision, Methodology, Investigation, Funding acquisition, Formal analysis, Conceptualization. **J.A. Almendros-Ibáñez:** Writing – review & editing, Supervision, Funding acquisition, Conceptualization. **D.C. Guío-Pérez:** Writing – review & editing, Supervision, Methodology, Investigation, Formal analysis, Data curation, Conceptualization.

Declaration of competing interest

The authors declare the following financial interests/personal relationships which may be considered as potential competing interests:

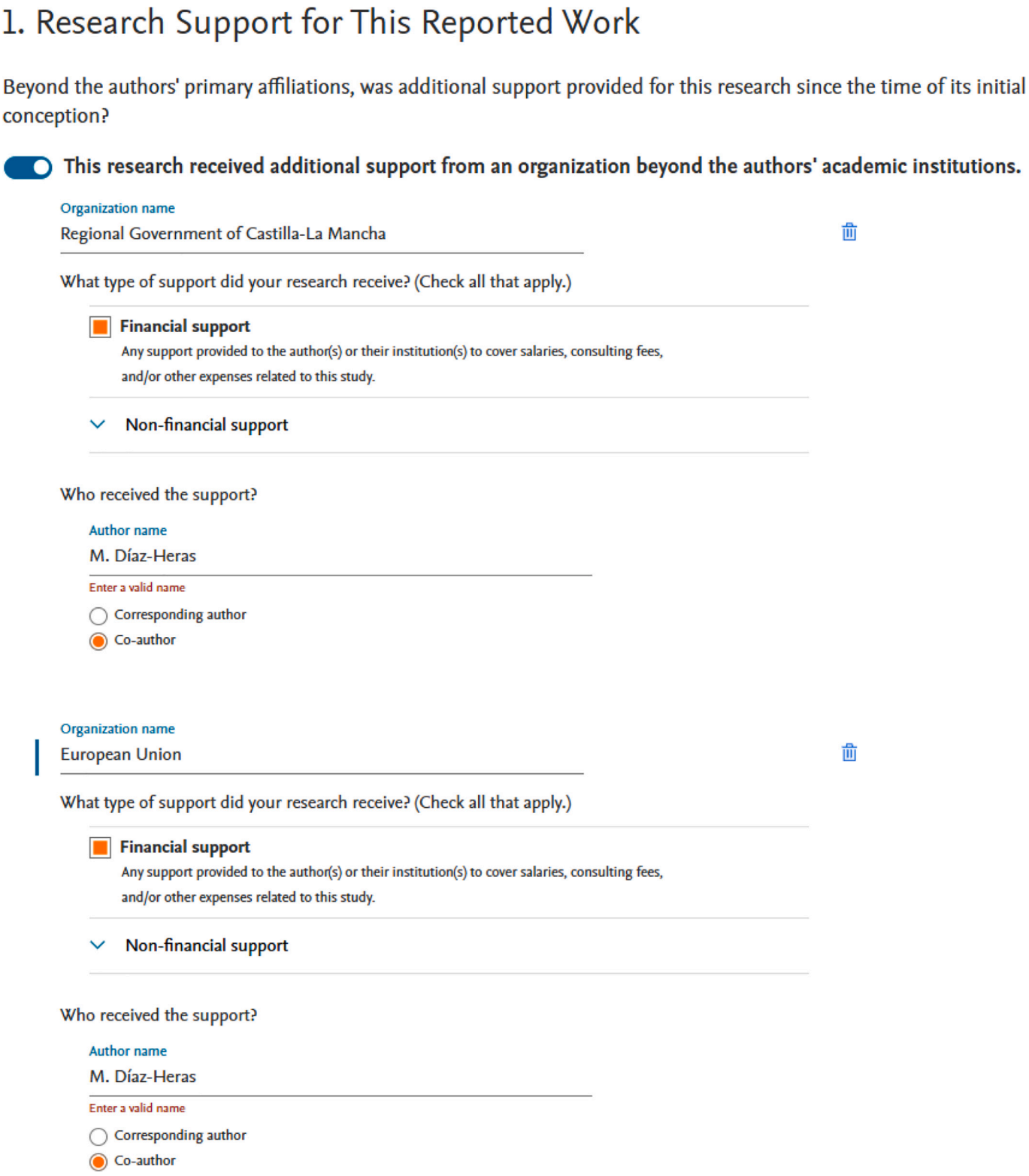

Acknowledgments

This work was partially funded by the project PID2024-159711OB-I00, CPP2023-010989 and RED2024-153629-T, by the Spanish Ministry of Science and Innovation MCIN/AEI/10.13039/5011000 11033/, by European Regional Development Fund "A way of making Europe", by European Union NextGenerationEU/PRTR, grant SBPLY/24/180225/000071, funded by the European Union through the ERDF and by the Regional Government of Castilla-La Mancha, Spain, through INNOCAM, and grant 2025-GRIN-38585, funded the University of Castilla-La Mancha, Spain. Minerva Díaz-Heras is grateful for the support of the 'UCLM mobility program' to facilitate research stays in universities and research centers abroad during the year 2024.

Data availability

Data will be made available on request.

References

[1] G.H. Reman, Effect of gas and solid mixing in fluidized beds on chemical reactions, Chem. Indust. (Lond. UK) (1955) 46–51.
[2] F. Wei, Y. Cheng, Y. Jin, Z. Yu, Axial and lateral dispersion of fine particles in a binary-solid riser, Can. J. Chem. Eng. 76 (1) (1998) 19–26, https://doi.org/10.1002/cjce.5450760104.
[3] A. Esin, M. Altun, Correlation of axial mixing of solids in fluidized beds by a dispersion coefficient, Powder Technol. 39 (3) (1984) 241–244, https://doi.org/10.1016/0032-5910(84)85041-X.
[4] W.J. Thiel, O.E. Potter, The mixing of solids in slugging gas fluidized beds, AICHE J. 24 (4) (1978) 561–569, https://doi.org/10.1002/aic.690240402.
[5] A. Avidan, J. Yerushalmi, Solids mixing in an expanded top fluid bed, AICHE J. 31 (5) (1985) 835–841, https://doi.org/10.1002/aic.690310520.
[6] E. Sette, D. Pallarès, F. Johnsson, Experimental evaluation of lateral mixing of bulk solids in a fluid-dynamically down-scaled bubbling fluidized bed, Powder Technol. 263 (2014) 74–80, https://doi.org/10.1016/j.powtec.2014.04.091.
[7] M. Stein, Y.L. Ding, J.P.K. Seville, D.J. Parker, Solids motion in bubbling gas fluidized beds, Chem. Eng. Sci. 55 (22) (2000) 5291–5300, https://doi.org/10.1016/S0009-2509(00)00177-9.
[8] H.R. Norouzi, N. Mostoufi, Z. Mansourpour, R. Sotudeh-Gharebagh, J. Chaouki, Characterization of solids mixing patterns in bubbling fluidized beds, Chem. Eng. Res. Des. 89 (6) (2011) 817–826, https://doi.org/10.1016/j.cherd.2010.10.014.
[9] L. Godfroy, J. Chaouki, F. Larachi, Position and velocity of a large particle in a gas/solid riser using the radioactive particle tracking technique, Can. J. Chem. Eng. 77 (1999) 253, https://doi.org/10.1002/cjce.5450770210.
[10] A. Köhler, D. Pallarès, F. Johnsson, Modeling axial mixing of fuel particles in the dense region of a fluidized bed, Energy Fuel 34 (3) (2020) 3294–3304, https://doi.org/10.1021/acs.energyfuels.9b04194.
[11] J.C. Abanades, G. Grasa, An extended version of the countercurrent back-mixing model suitable for solid mixing in two-dimensional fluidized beds, Powder Technol. 118 (1–2) (2001) 180–187, https://doi.org/10.1016/S0032-5910(01)00357-6.
[12] S. Migliozzi, A. Paulillo, R. Chirone, P. Salatino, R. Solimene, Hydrodynamics of compartmented fluidized beds under uneven fluidization conditions, Powder Technol. 316 (2017) 476–491, https://doi.org/10.1016/j.powtec.2016.12.052.
[13] J. Cardoso, V. Silva, D. Eusébio, P. Brito, R.M. Boloy, L. Tarelho, J.L. Silveira, Comparative 2D and 3D analysis on the hydrodynamics behaviour during biomass gasification in a pilot-scale fluidized bed reactor, Renew. Energy 131 (2019) 713–729, https://doi.org/10.1016/j.renene.2018.07.080?utm_source=chatgpt.com.
[14] G. Grasa, J.C. Abanades, The use of two different models to describe the axial mixing of solids in fluidised beds, Chem. Eng. Sci. 57 (14) (2002) 2791–2798, https://doi.org/10.1016/S0009-2509(02)00146-X.
[15] P. Salatino, P. Ammendola, P. Bareschino, R. Chirone, R. Solimene, Improving the thermal performance of fluidized beds for concentrated solar power and thermal energy storage, Powder Technol. 290 (2016) 97–101, https://doi.org/10.1016/j.powtec.2015.07.036.
[16] X. Yupeng, L. Tingwen, L. Liqiang, X. Gao, S. Tebianian, J. Grace, J. Chaouki, T. Leadbeater, R. Jafari, D. Parker, J. Seville, N. Ellis, Development and confirmation of a simple procedure to measure solids distribution in fluidized beds using tracer particles, Chem. Eng. Sci. 217 (2020) 115501, https://doi.org/10.1016/j.ces.2020.115501.
[17] A. Bakshi, A.F. Ghoniem, C. Altantzis, Mixing dynamics in bubbling fluidized beds, AICHE J. 63 (10) (2017) 4316–4328, https://doi.org/10.1002/aic.15801.
[18] J.A. Medrano, M. Tasdemir, F. Gallucci, M. van Sint Annaland, On the internal solids circulation rates in freely-bubbling gas-solid fluidized beds, Chem. Eng. Sci. 172 (2017) 395–406, https://doi.org/10.1016/j.ces.2017.06.046.
[19] P.N. Rowe, B.A. Partridge, A.G. Cheney, G.A. Henwood, E. Lyall, The mechanisms of solids mixing in fluidised beds, Chem. Eng. Res. Des. 43a (1965) 271–286.
[20] L.R. Glicksman, M. Hyre, K. Woloshun, Simplified scaling relationships for fluidized beds, Powder Technol. 77 (2) (1993) 177–199, https://doi.org/10.1016/0032-5910(93)80036-U.
[21] M. Díaz-Heras, J.F. Belmonte, J.A. Almendros-Ibáñez, Experimental observations on directly irradiated fluidized beds: even and uneven fluidization, Exp. Thermal Fluid Sci. 120 (2021) 110242.
[22] A. Köhler, E. Cano-Pleite, A. Soria-Verdugo, D. Pallarès, F. Johnsson, Modeling the motion of fuel particles in a fluidized bed, Fuel 305 (2021) 121424, https://doi.org/10.1016/j.fuel.2021.121424.
[23] R.C. Darton, R.D. LaNauze, J.F. Davidson, D. Harrison, Bubble growth due to coalescence in fluidized beds, Trans. Inst. Chem. Eng. 55 (1977) 274–280.
[24] J.F. Davidson, D. Harrison, Fluidized Particles, Cambridge University Press, Cambridge, 1963.